This article has been accepted for publication in a future issue of this journal, but has not been fully edited. Content may change prior to final publication. Citation information: DOI 10.1109/TPWRD.2018.2847725, IEEE Transactions on Power Delivery

A Damping Factor-Based White-Box Transformer Model for Network Studies

Bjørn Gustavsen, *Fellow, IEEE* and Álvaro Portillo, *Senior Member, IEEE*

***Abstract*—Transformer manufacturers make routine use of white-box detailed transformer models for ensuring that the transformer will pass the lightning impulse test. For use in general simulation studies, the model should additionally be multi-phase and properly reproduce the transformer's input impedance characteristics and voltage ratios at 50/60 Hz. One challenge in such general modeling scope is to properly represent the frequency-dependent damping of the transformer's many resonances. In this work we show how to properly include empirical damping factors in a multi-phase admittance-based formulation of the state-equations. It is shown that the substitution of the real part of the state matrix eigenvalues causes some undesired changes to the model's behavior at lower frequencies, but this deficiency is mitigated by a correction to the output matrix. The resulting model can be directly included in EMTP-type simulation programs via a companion model, or via a terminal model with an add-on model for optional calculation of selected internal node voltages. Application of the modeling approach to a single-phase three-winding transformer demonstrates its merit in terms of accuracy and efficiency. Finally, the limitations of the model are discussed regarding accuracy and applications scope.**

***Index Terms*—Transformer, White box model, EMTP, Simulation.**

I. Introduction

TRANSFORMER manufacturers apply dedicated computational tools for assessing the dielectric stresses inside windings due to factory test with the lightning impulse voltage [1]. The calculations are performed using so-called white-box transformer models [2], [3] where the windings are modeled in detail, typically using lumped parameter type models, or transmission line models.

There is an increasing interest in utilizing the manufacturer's white-box models in EMTP-type circuit simulators for studies of high-frequency interactions between transformers and the system. The lumped parameter type models involve a circuit of coupled RLC elements which can in principle be directly imported into EMTP-type tools; however, the manufacturers are sometimes reluctant to sharing such detailed models with a customer. The authors recently proposed [4] an alternative state space-based approach for interfacing such models with EMTP tools which permits the manufacturer to conceal information about internal voltages. A different approach [5] is to calculate admittance parameters with respect to external nodes in the frequency domain, and fit a black-box model to the data via curve fitting. Internal voltages can be simulated via a rational function model of the voltage transfer function from the external nodes to all internal nodes. Such approach can also include the frequency-dependency in the parameters [6], but the its accurate determination can be challenging.

In practice it can be difficult to determine the losses in the transformer as function of frequency and thereby the values of the matrices of series resistance **R** and shunt conductance **G**. In the *k*-factor approach [4], the resistances are chosen equal to dc values and scaled with an appropriate (large) value to give an acceptable agreement with observed voltage wave shapes. However, this method leads to large errors at 50/60 Hz due to overdamping, limiting the scope of the model. A different approach was taken in [7], based on a state-space model with voltage application on one terminal as input and voltage response on internal winding points as outputs. The real parts of the state matrix eigenvalues were substituted with frequency-dependent empirical values obtained from observation of transient responses. This damping approach method is commonly applied among manufacturers for assessing the winding voltage distribution during the lightning impulse test.

In this work we introduce the damping factor in a multi-port state-space model of the transformer. That formulation has current injection as input and voltage response as output, thereby including information about the terminal input impedance, unlike the voltage transfer formulation in the original damping factor approach [7]. Based on a consideration of how the damping factor affects the model's accuracy via its points of resonance and anti-resonance, we modify the state-space model such that the input is applied voltage on external terminals while the response is current on external terminals and voltage on internal nodes. We next introduce the empirical damping factor into the eigenvalues of the state matrix, thereby achieving frequency-dependent attenuation of the modes, leading to a *d*-factor model. A correction factor is introduced which mitigates undesired changes to the model's behavior at

Manuscript received December 29, 2017,…

B. Gustavsen is with SINTEF Energy Research, N-7465 Trondheim, Norway (e-mail: bjorn.gustavsen@sintef.no).

Á. Portillo is an independent consultant in transformers, Brenda 5920, 11400, Montevideo, Uruguay (e-mail: acport18@gmail.com).

This article has been accepted for publication in a future issue of this journal, but has not been fully edited. Content may change prior to final publication. Citation information: DOI 10.1109/TPWRD.2018.2847725, IEEE Transactions on Power Delivery

low frequencies that are caused by the damping factor. The interfacing of the model with EMTP-type circuit simulators is described in some detail. The modeling approach is demonstrated for a single-phase three-winding transformer and simulation results are compared against actual measurements.

II. Damping Factor Method

A. Damping Factor

For calculation of internal oscillations in transformer windings it has been proposed [7] to use an experimentally obtained damping function (1) which relates resonance frequency (β) and damping (α),

$$\alpha = f(\beta) \tag{1}$$

The damping function was obtained from samples $(\alpha_i + j\beta_i)$ associated with observed voltage oscillations [7],

$$y(t) = \sum_i k_i e^{\alpha_i t} \cos(\beta_i t + \theta_i) \tag{2}$$

The samples $(\alpha_i + j\beta_i)$ are also the eigenvalues of a corresponding state equation. It is further observed that (α/β) defines the damping *factor* of the oscillation, i.e. by which factor each of the natural oscillations is scaled down by damping effects.

In the work [7], measurements were performed on 25 transformers of different sizes, giving the damping factor (3). Here, ω represents the eigenvalue imaginary part, β.

$$(\frac{\alpha}{\omega}) = -(0.022 + 0.058 \cdot 10^{-6} \cdot \omega)\,,\ \omega \le 5 \cdot 10^5 \tag{3a}$$

$$(\frac{\alpha}{\omega}) = -0.050\,,\ \omega > 5 \cdot 10^5 \tag{3b}$$

B. Uniqueness

Consider a linear model with input u and output y. In the frequency domain we can write

$$y(s) = H(s) \cdot u(s) \tag{4}$$

The transfer function H can be expressed on alternative forms, by a state-space model (5a), a pole-residue model (5b) and pole-zero model (5c).

$$H(s) = \mathbf{c}^T (s\mathbf{I} - \mathbf{A})^{-1}\mathbf{b} + d \tag{5a}$$

$$H(s) = d + \sum_i \frac{r_i}{s - a_i} \tag{5b}$$

$$H(s) = K \frac{\prod_j (s - z_j)}{\prod_i (s - a_i)} \tag{5c}$$

The complex poles and zeros in (5) appear as conjugate pairs. With the damping factor method, one replaces the real part of each complex pole by a different value according to some (empirical) function via (1),

$$a_i = \alpha_i \pm j\beta_i \ \rightarrow\ \bar{a}_i = \bar{\alpha}_i \pm j\beta_i \tag{6}$$

It follows that the damping function affects the state matrix **A** and the poles a_i, while the other coefficients remain unchanged. Consider that one interchanges input and output in (4). One observes from (5c) that the poles and zeros of the original model respectively become zeros and poles in the new model. This tells us that the damping factor is not unique in the sense that its impact on the model's behavior depends on the choice of input and output. For instance, if the original model represents admittance, the voltage is input. This model will with a current application give a different result than an impedance-based model with current application, when the eigenvalues of each model have been modified by a damping function (3). This consideration to uniqueness can be generalized to multi-port systems as the poles are the eigenvalues of **A**. It follows that the choice of input and output variables for a white-box transformer model is not arbitrary.

III. State-Space Modeling

A. Circuit Equations

We consider a lumped-parameter white-box model of a transformer with spatial discretization of its windings. The fundamental equations defining the electrical behavior was described in [4] but is briefly repeated here. The basic equations related to the circuit parameters (matrices) **R**, **L**, **C**, **G** is defined by (7), (8), and (9). The model has N nodes and M branches. Variables **v**, **i** and **e** denote node voltages, inductive branch currents, and inductive branch voltages.

$$\mathbf{i}_C = \mathbf{C}\dot{\mathbf{v}} \tag{7}$$

$$\mathbf{i}_G = \mathbf{G}\mathbf{v} \tag{8}$$

$$\mathbf{e} = \mathbf{L}\dot{\mathbf{i}} + \mathbf{R}\mathbf{i} \tag{9}$$

An incidence matrix **T** (10), dependent on internal connections, is used for relating node voltages **v** with inductive branch voltages **e**, and for relating the inductive branch currents **i** with the sum $\mathbf{i}_L$ of all inductive branch currents flowing out of branch nodes,

$$\mathbf{e} = \mathbf{T}\mathbf{v} \tag{10}$$

$$\mathbf{i}_L = \mathbf{T}^T\mathbf{i} \tag{11}$$

At each node, the total $\mathbf{i}_S$ current flowing into each node is

$$\mathbf{i}_C + \mathbf{i}_L + \mathbf{i}_G = \mathbf{i}_S \tag{12}$$

Introducing (7), (8), (10) and (11) in (12) and (9) gives:

$$\mathbf{C}\dot{\mathbf{v}} = -\mathbf{G}\mathbf{v} - \mathbf{T}^T\mathbf{i} + \mathbf{i}_S \tag{13}$$

$$\mathbf{L}\dot{\mathbf{i}} = \mathbf{T}\mathbf{v} - \mathbf{R}\mathbf{i} \tag{14}$$

B. State-Space Model

The above equations can be combined into the state equation (15) as

This article has been accepted for publication in a future issue of this journal, but has not been fully edited. Content may change prior to final publication. Citation information: DOI 10.1109/TPWRD.2018.2847725, IEEE Transactions on Power Delivery

$$\begin{bmatrix}\dot{\mathbf{v}}\\ \dot{\mathbf{i}}\end{bmatrix}=\begin{bmatrix}-\mathbf{C}^{-1}\mathbf{G} & -\mathbf{C}^{-1}\mathbf{T}^{T}\\ \mathbf{L}^{-1}\mathbf{T} & -\mathbf{L}^{-1}\mathbf{R}\end{bmatrix}\cdot\begin{bmatrix}\mathbf{v}\\ \mathbf{i}\end{bmatrix}+\begin{bmatrix}\mathbf{C}^{-1} & \mathbf{0}\\ \mathbf{0} & \mathbf{0}\end{bmatrix}\begin{bmatrix}\mathbf{i}_S\\ \mathbf{0}\end{bmatrix} \quad (15)$$

Connections between nodes and grounding of nodes is achieved by a modification of matrices **C**, **G** and **T** based on the procedure described in the Appendix of [4].

For convenience we introduce the reordering matrix **Q** which makes the external n_1 nodes come first and the internal n_2 nodes last (n_1+n_2=N) via the relations (16).

$$\bar{\mathbf{v}}=\mathbf{Q}\mathbf{v}\,,\quad \bar{\mathbf{i}}_S=\mathbf{Q}\mathbf{i}_S\,,\quad \mathbf{Q}^{-1}=\mathbf{Q}^{T} \quad (16)$$

The state-space model (15) becomes

$$\begin{bmatrix}\dot{\bar{\mathbf{v}}}\\ \dot{\mathbf{i}}\end{bmatrix}=\begin{bmatrix}-\mathbf{Q}\mathbf{C}^{-1}\mathbf{G}\mathbf{Q}^{T} & -\mathbf{Q}\mathbf{C}^{-1}\mathbf{T}^{T}\\ \mathbf{L}^{-1}\mathbf{T}\mathbf{Q}^{T} & -\mathbf{L}^{-1}\mathbf{R}\end{bmatrix}\cdot\begin{bmatrix}\bar{\mathbf{v}}\\ \mathbf{i}\end{bmatrix}+\begin{bmatrix}\mathbf{Q}\mathbf{C}^{-1}\mathbf{Q}^{T}\\ \mathbf{0}\end{bmatrix}\bar{\mathbf{i}}_S \quad (17)$$

C. Modifying Input and Output Variables

The transformer input impedance at high frequencies is usually high as compared to the components to which it is connected, e.g. the characteristic impedance of cables and overhead lines. The transformer terminals are therefore subjected to voltage applications rather than current applications. From the reasoning in Section II.B it follows that it can be advantageous to base the model on a formulation with voltage as input instead of current.

The notation for (17) is first simplified by partitioning the variables according to external voltages/currents. This gives for the complete state space model,

$$\begin{bmatrix}\dot{\mathbf{v}}_{\text{ext}}\\ \dot{\mathbf{x}}_2\end{bmatrix}=\begin{bmatrix}\mathbf{A}_1 \,\vdots\, \mathbf{A}_2\end{bmatrix}\cdot\begin{bmatrix}\mathbf{v}_{\text{ext}}\\ \mathbf{x}_2\end{bmatrix}+\begin{bmatrix}\mathbf{B}_1 \,\vdots\, \mathbf{B}_2\end{bmatrix}\begin{bmatrix}\mathbf{i}_{\text{ext}}\\ \mathbf{u}_2\end{bmatrix} \quad (18a)$$

$$\begin{bmatrix}\mathbf{v}_{\text{ext}}\\ \mathbf{x}_2\end{bmatrix}=\begin{bmatrix}\mathbf{I}_{\text{ext}} & \mathbf{0}\\ \mathbf{0} & \mathbf{I}_2\end{bmatrix}\cdot\begin{bmatrix}\mathbf{v}_{\text{ext}}\\ \mathbf{x}_2\end{bmatrix} \quad (18b)$$

We next introduce resistors in series with the external terminals as shown in Fig. 1. Each resistance should be a small fraction of the DC resistance of the associated winding.

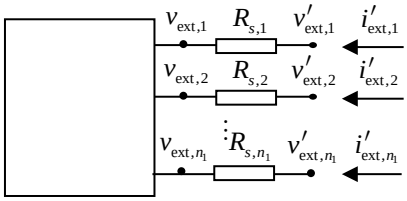

Fig. 1. Introducing resistors in series with transformer's external terminals.

For the series connection in Fig. 1 we can write

$$\mathbf{i}'_{\text{ext}}=\mathbf{G}_{\text{ext}}(\mathbf{v}'_{\text{ext}}-\mathbf{v}_{\text{ext}}) \quad (19)$$

where $\mathbf{G}_{\text{ext}}$ is a diagonal matrix holding the inverse of the resistor elements in Fig. 1, $G_{\text{ext}}(i,i)=1/R_{s,i}$, $i=1\ldots n_1$. Introducing (19) in (18) and noting that $\mathbf{u}_2$=**0** gives a new state-space model,

$$\begin{bmatrix}\dot{\mathbf{v}}_{\text{ext}}\\ \dot{\mathbf{x}}_2\end{bmatrix}=\begin{bmatrix}(\mathbf{A}_1-\mathbf{B}_1\mathbf{G}_{\text{ext}}) \,\vdots\, \mathbf{A}_2\end{bmatrix}\cdot\begin{bmatrix}\mathbf{v}_{\text{ext}}\\ \mathbf{x}_2\end{bmatrix}+\begin{bmatrix}\mathbf{B}_1\mathbf{G}_{\text{ext}}\end{bmatrix}\mathbf{v}'_{\text{ext}} \quad (20a)$$

$$\begin{bmatrix}\mathbf{i}'_{\text{ext}}\\ \mathbf{x}_2\end{bmatrix}=\begin{bmatrix}-\mathbf{G}_{\text{ext}} & 0\\ \mathbf{0} & \mathbf{I}_2\end{bmatrix}\cdot\begin{bmatrix}\mathbf{v}_{\text{ext}}\\ \mathbf{x}_2\end{bmatrix}+\begin{bmatrix}\mathbf{G}_{\text{ext}}\\ \mathbf{0}\end{bmatrix}\mathbf{v}'_{\text{ext}} \quad (20b)$$

It is observed that in this model, external voltage $\mathbf{v}'_{\text{ext}}$ is input and external current $\mathbf{i}'_{\text{ext}}=\mathbf{i}_{\text{ext}}$ is output. As will be shown in Section IX.A, the change of variable has the advantage that the large eigenvalues of the terminal admittance matrix at 50/60 Hz becomes much less affected by the damping factor which is introduced in Section IV.

IV. Damping Factor Method

A. Inclusion of Damping Factor in State Space Model

To simplify notation, we write (20) on standard form,

$$\begin{aligned}\dot{\mathbf{x}}&=\mathbf{A}\mathbf{x}+\mathbf{B}\mathbf{u}\\ \mathbf{y}&=\mathbf{C}\mathbf{x}+\mathbf{D}\mathbf{u}\end{aligned} \quad (21)$$

The state matrix of the model (21) is subjected to diagonalization by eigenvector decomposition,

$$\mathbf{A}=\mathbf{S}\tilde{\mathbf{A}}\mathbf{S}^{-1} \quad (22)$$

Since **A** is a real matrix, its eigenvalues and associated eigenvectors are real or come in complex conjugate pairs. Each complex eigenvalue

$$\lambda_i=\alpha_i\pm j\beta_i \quad (23)$$

has its real part replaced with the empirical value given by (1),

$$\bar{\alpha}_i\leftarrow f(\beta_i) \quad (24)$$

where f is the damping function. In the case that the original eigenvalues represent a system with losses ignored or greatly underestimated (e.g. calculated at 50/60 Hz), β is effectively the undamped resonance frequency. To obtain the damped resonance frequency we update β,

$$\bar{\beta}_i\leftarrow\sqrt{\beta_i^2-\bar{\alpha}_i^2} \quad (25)$$

The substitutions (24) and (25) lead to a modified state matrix in (21),

$$\bar{\mathbf{A}}=\mathbf{A}+\Delta\mathbf{A} \quad (26)$$

B. Recovering Accuracy at 50/60 Hz

As will be shown in Section VII, the replacement of **A** with $\bar{\mathbf{A}}$ causes the low-frequency behavior of the terminal admittance matrix to change at lower frequencies. The change to the input-output transfer function **H** (5a) due to (26) is in the frequency domain given as

$$\mathbf{H}(s)=\mathbf{C}(\mathbf{sI}-\mathbf{A})^{-1}\mathbf{B}\rightarrow\hat{\mathbf{H}}(s)=\mathbf{C}(\mathbf{sI}-\bar{\mathbf{A}})^{-1}\mathbf{B} \quad (27)$$

In order to retain the original behavior at low frequencies, we enforce the condition that the change to **H** at 50/60 Hz is zero. Denoting this frequency (50/60 Hz) as s_0 we introduce an unknown scaling matrix **F** so that

$$\mathbf{C}\mathbf{F}(s_0\mathbf{I}-\bar{\mathbf{A}})^{-1}\mathbf{B}=\mathbf{C}(s_0\mathbf{I}-\mathbf{A})^{-1}\mathbf{B} \quad (28)$$

This article has been accepted for publication in a future issue of this journal, but has not been fully edited. Content may change prior to final publication. Citation information: DOI 10.1109/TPWRD.2018.2847725, IEEE Transactions on Power Delivery

whose solution is

$$\mathbf{F} = (s_0\mathbf{I} - \mathbf{A})^{-1}(s_0\mathbf{I} - \bar{\mathbf{A}}) \tag{29}$$

F has a small imaginary part which is undesirable as it prevents a real-valued realization of the final state space model. This difficulty is avoided by first expressing **F** on its diagonal form (30a), (30b), see proof in Appendix.

$$\mathbf{F}(s) = \mathbf{S}\boldsymbol{\Lambda}\mathbf{S}^{-1} \tag{30a}$$

$$\lambda_i = \frac{s_0 - \bar{a}_i}{s_0 - a_i} = \lambda_i' + j\lambda_i'' \tag{30b}$$

A real-valued **F** is achieved by enforcing that its eigenvalues (30b) are real or complex conjugate, compliant with the columns of **S** and rows of $\mathbf{S}^{-1}$. The complex pairs are identified via the eigenvalues of the original state matrix **A**. For any complex pair

$$(\lambda_i' + j\lambda_i''),\ (\lambda_{i+1}' - j\lambda_{i+1}'') \tag{31}$$

the following substitutions are made via averaging,

$$\lambda_i' = \lambda_{i+1}' \leftarrow \frac{\lambda_i' + \lambda_{i+1}'}{2},\ \lambda_i'' = \lambda_{i+1}'' \leftarrow \frac{\lambda_i'' + \lambda_{i+1}''}{2} \tag{32}$$

With the modified eigenvalues (32), the real-valued **F** is calculated via (30a) which gives the final state space model

$$\begin{aligned} \dot{\mathbf{x}} &= \bar{\mathbf{A}}\mathbf{x} + \mathbf{B}\mathbf{u} \\ \mathbf{y} &= (\mathbf{CF})\mathbf{x} + \mathbf{D}\mathbf{u} \end{aligned} \tag{33}$$

V. Direct Interfacing With Circuit Simulators

The model (33) can be directly interfaced with circuit simulation programs via its admittance parameter representation, defined by the first n_1 elements of **u** ($\mathbf{v}_{\text{ext}}'$) and first n_1 elements of **y** ($\mathbf{i}_{\text{ext}}'$). In order to achieve high computational efficiency in a time domain simulation, it is necessary to utilize the state equation on its diagonal form. This gives for (33),

$$\begin{aligned} \dot{\tilde{\mathbf{x}}} &= \tilde{\bar{\mathbf{A}}}\tilde{\mathbf{x}} + \mathbf{S}^{-1}\mathbf{B}\mathbf{u} \\ \mathbf{y} &= (\mathbf{CFS})\tilde{\mathbf{x}} + \mathbf{D}\mathbf{u} \end{aligned} \tag{34}$$

The actual implementation is similar to that of the *k*-factor model in [4] by use of a Norton-type companion model in combination with recursive convolution. The model optionally gives out the internal node voltages by including the corresponding rows of **CFS** in the model.

VI. Alternative Interfacing Approach

Most EMTP-type circuit simulators lack the capability of direct inclusion of the model (34) with proper utilization of the sparse structure. Until such capability is made available, it is possible to do the interfacing with a pole-residue model that represents external terminals and an optional voltage transfer block that gives the voltage on selected internal nodes. The voltage transfer can also be implemented as an offline model in a separate program, e.g. Matlab.

A. External Terminals

The model is interfaced via a pole-residue model that represents the terminal behavior only. This model is obtained by calculating frequency samples for the terminal admittance matrix $\mathbf{Y}_{\text{ext}}(s_k)$ that is subjected to least squares rational fitting and passivity enforcement [8] by the (symmetrical) model

$$\mathbf{Y}_{\text{ext}}(s_k) \cong \mathbf{R}_0 + \sum_i \frac{\mathbf{R}_i}{s_k - a_i},\ k = 1 \ldots N_s \tag{35}$$

The calculation of samples of $\mathbf{Y}_{\text{ext}}(s_k)$ is done in a robust and efficient manner by utilizing the diagonal form (34) of the state-space matrix. When also replacing **F** by its diagonal form (30a), one gets

$$\mathbf{Y}_{\text{ext}}(s) = (\mathbf{CS})_{\text{sub}} \cdot \mathbf{E}(s) \cdot (\mathbf{S}^{-1}\mathbf{B}) + \mathbf{G}_{\text{ext}} \tag{36a}$$

where $(\mathbf{CS})_{\text{sub}}$ denotes the first n_1 rows of **CS**,

$$(\mathbf{CS})_{\text{sub}} = (\mathbf{CS})(1\!:\!n_1,:) \tag{36b}$$

E(*s*) is a diagonal matrix with elements

$$e_{ii}(s)\frac{\lambda_i}{s - \bar{a}_i} \tag{36c}$$

where λ_i, and $\bar{a}_i$ are the eigenvalues of **F** and $\bar{\mathbf{A}}$, respectively.

When internal connections and grounding of nodes are handled as in this work (see Appendix in [4]), the state matrix **A** gets one or more zero eigenvalues. The zero eigenvalues are removed by deleting corresponding entries in **E**, and ditto columns of **CS** and rows of $\mathbf{S}^{-1}\mathbf{B}$.

B. Internal Node Voltages and Branch Currents

The internal node voltages and branch currents are obtained via models $\mathbf{J}_1$ and $\mathbf{J}_2$,

$$\mathbf{v}_{\text{int}}(s) = \mathbf{J}_1(s) \cdot \mathbf{v}_{\text{ext}}'(s) \tag{37a}$$

$$\mathbf{i}_{\text{branch}}(s) = \mathbf{J}_2(s) \cdot \mathbf{v}_{\text{ext}}'(s) \tag{37b}$$

where

$$\mathbf{J}_1(s) = (\mathbf{CS})(n_1 : N_1,:) \cdot \mathbf{E}(s) \cdot (\mathbf{S}^{-1}\mathbf{B}) \tag{38a}$$

$$\mathbf{J}_2(s) = (\mathbf{CS})(N+1\!:\!N+M,:) \cdot \mathbf{E}(s) \cdot (\mathbf{S}^{-1}\mathbf{B}) \tag{38b}$$

$\mathbf{J}_1$ and $\mathbf{J}_2$ are in (38a) and (38b) seen to be calculated using different rows of **CS**, from n_1 to N_1 and from N_1+1 to N+M, respectively.

C. Time Domain Simulation

In a time domain simulation, the pole-residue model (35) is interfaced with the circuit simulator by recursive convolution via a Norton equivalent as described in [9]. The simulation gives in each time point t_k the voltage $\mathbf{v}_{\text{ext}}'(t_k)$ on the transformer external terminals.

For calculation of internal node voltages and branch currents, the model (38) is interfaced with the circuit simulator as a state-

This article has been accepted for publication in a future issue of this journal, but has not been fully edited. Content may change prior to final publication. Citation information: DOI 10.1109/TPWRD.2018.2847725, IEEE Transactions on Power Delivery

space model on diagonal form with usage of recursive convolution, with the calculated value for $\mathbf{v}'_{\text{ext}}(t_k)$ as input,

$$\mathbf{v}_{\text{int}}(t) = J_1(t) * \mathbf{v}'_{\text{ext}}(t) \tag{39a}$$

$$\mathbf{i}_{\text{branch}}(t) = J_2(t) * \mathbf{v}'_{\text{ext}}(t) \tag{39b}$$

The convolutions (39a) and (39b) can be performed off-line since they do not interact with the system.

VII. Application to Single-Phase Transformer

A. Transformer

We consider a single-phase three-winding transformer as shown in Fig. 2. This is a 50 MVA unit with rated voltage $230/\sqrt{3}$, $69/\sqrt{3}$, 13.8 kV at 60 Hz. The core has one mid-leg and two return legs.

B. White-Box Modeling

A white-box lumped parameter type model is calculated via spatial discretization and analytical formulae following a similar approach as in [4]. The model has N=219 nodes and M=213 inductive branches. Terminals H1, X1, Y1 and Y2 are treated as external terminals, giving n_1=4. Terminals H0 and X0 are grounded. The calculations are performed with a k-factor k=1, i.e. using DC resistances.

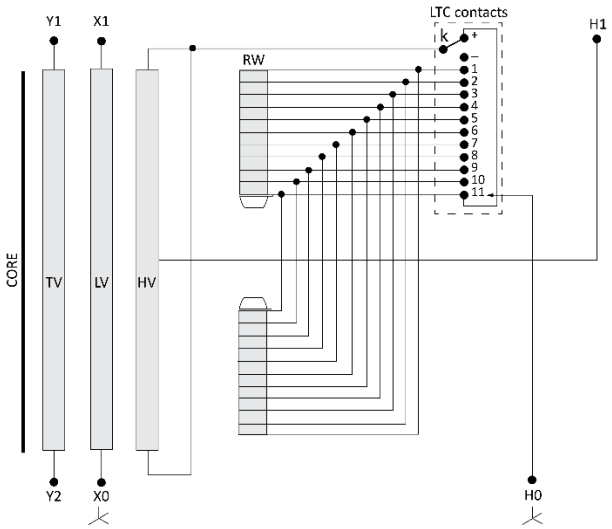

Fig. 2. Single phase transformer with external terminals and internal connections.

C. Damping Function

A suitable damping curve can be extracted directly from the measured frequency domain responses via rational fitting [10]. For the given transformer, several voltage transfer measurements were performed [11]. As an example, we consider the measured voltage response to two alternative voltage applications as shown in Table I. The tap setting is in middle position.

TABLE I
VOLTAGE TRANSFER MEASUREMENTS.

Case	Voltage applied on	Grounded terminals	Voltage response on
6	H1	H0, X0	X1, Y1, Y2
38	X1	H0, X0	H1, Y1, Y2

The responses are fitted using a high-order common pole set as shown in Fig. 3. From the extracted poles, a damping function (40) is calculated based on the extracted poles using least squares approximation, see Fig. 4. The model has parameters a=–0.00590, b=0.9762. The damping function is in Fig. 4 compared to the one (3) in [7] denoted "Fergestad", showing a remarkably good agreement above $5\cdot10^5$ rad/sec. Below this frequency, the Fergestad curve gives too low damping.

The state matrix **A** is diagonalized (22) and the eigenvalues are modified by the damping function (40) via (24) and (25), using the calculated (fitted) model in Fig. 4.

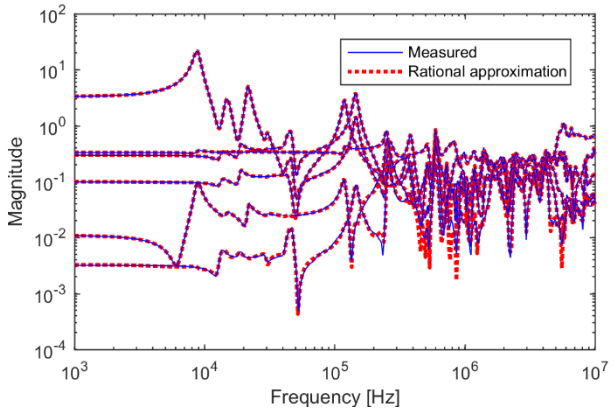

Fig. 3. Fitting the voltage transfer functions with a rational model.

$$\alpha = a \cdot \omega^b \tag{40}$$

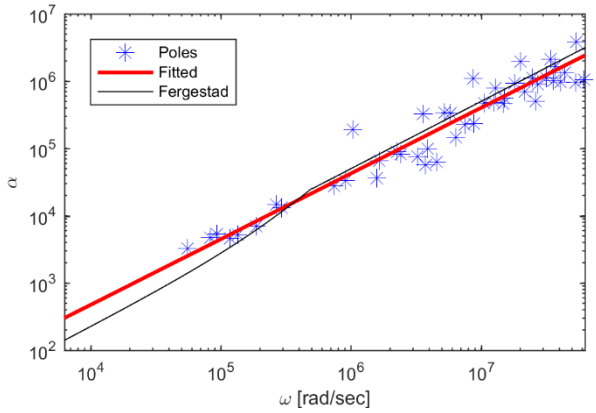

Fig. 4. Damping curve for extracted poles.

D. Core Losses

The white-box model used as starting point in Section VII.B includes an inductive core equivalent by the approach described in Appendix in [4]. In addition, we add a resistor between Y1 and Y2 which represents the no-load losses. This resistor R is added externally to the model, after introduction of the damping factor. Since the associated hysteresis losses are not present at high frequencies, we add a series inductance L to block the loss

This article has been accepted for publication in a future issue of this journal, but has not been fully edited. Content may change prior to final publication. Citation information: DOI 10.1109/TPWRD.2018.2847725, IEEE Transactions on Power Delivery

effect at high frequencies. The inductance is chosen such that $\omega L=R$ at 1 kHz.

E. Terminal Admittance Matrix

The terminal admittance matrix $\mathbf{Y}_{\text{ext}}$ is calculated using the approach described in Section VI-A, with R_s=1 mΩ. In order to recover the original behavior at low frequencies, the matrix **F** (29) is utilized with $s_0 = j2\pi \cdot 60$. Fig. 5 shows the resulting 16 elements of $\mathbf{Y}_{\text{ext}}$, before and after introduction of the damping factor. It is observed that the resulting model preserves the original behavior at low frequencies and that it gives a strong damping of the resonance peaks at higher frequencies.

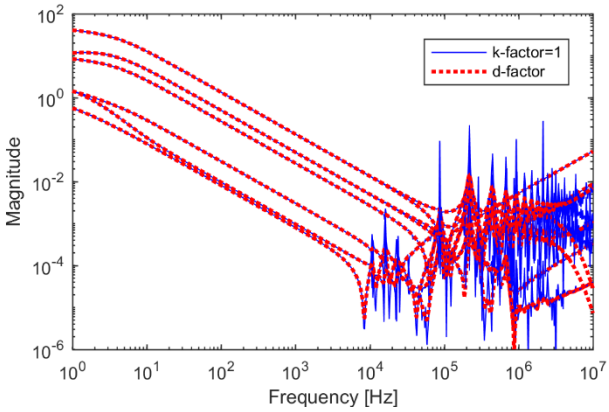

Fig. 5. Impact of damping function on terminal admittance matrix.

The improvement by introducing **F** (29) is highlighted in Fig. 6 which shows the eigenvalues of $\mathbf{Y}_{\text{ext}}$. It is observed that by usage of **F**, the original behavior of the two small eigenvalues of $\mathbf{Y}_{\text{ext}}$ is recovered at low frequencies. These eigenvalues are respectively associated with the no-load currents and the tertiary winding common mode capacitive charging current. The large eigenvalues are virtually unaffected by **F** since they were not noticeably affected by the damping factor. At higher frequencies, the resonance peaks appear unchanged while the anti-resonance peaks are more damped. Table II shows the impact of using **F** on the voltage ratios X/H and X/T, as well as the short-circuit and open-circuit impedance seen from terminal H at 60 Hz. It is observed that the impact of the damping factor is negligible on the voltage ratio and on the short-circuit impedance while it has a large impact on the open-circuit impedance. However, with usage of **F** also the open circuit impedance becomes close to that in the original value.

The last row in Table II shows the corresponding data from the transformer's Factory Acceptance Test (FAT), taken as the average of seven sister units. The impedances, losses and currents are referred to the high-voltage side. The agreement between calculations and FAT results is seen to be very good, except for the no-load current. The reason for the deviation in no-load current is that the applied common flux inductance L_0 as defined in Appendix A in [4] is too small in the white-box model, which was calculated prior to the measurements. By increasing the inductance from L_0=0.582 mH to L_0=2.2 mH, a very good accuracy is achieved for the no-load current as well.

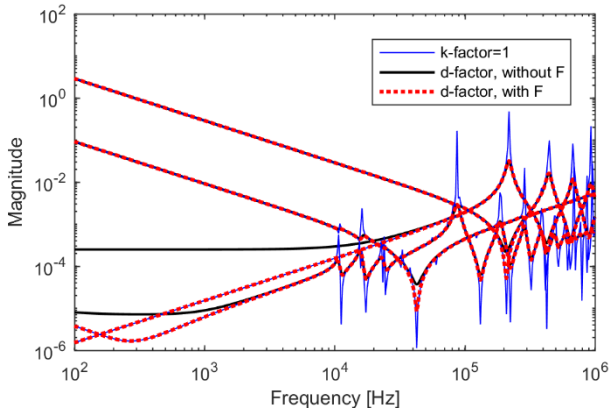

Fig. 6. Eigenvalues of $\mathbf{Y}_{\text{ext}}$, with and without usage of **F**.

TABLE II
VOLTAGE RATIOS, SHORT-CIRCUIT IMPEDANCE, OPEN-CIRCUIT LOSSES AND CURRENT.

	V_S/V_P	V_T/V_P	Z_k [Ω]	P_{oc} [kW]	I_{oc} [A]
Original model	0.300	0.104	1.51+j74.4	33.4	0.93
Model with *d*-factor	0.300	0.104	1.55+j74.4	140.1	1.38
Model with *d*-factor and **F**	0.300	0.104	1.51+j74.4	33.4	0.93
FAT	0.300*	0.104*	1.50+j75.1	33.0	0.32

*Calculated from turns ratio

F. Model Extraction

The terminal admittance matrix $\mathbf{Y}_{\text{ext}}$ (with usage of **F**) is subjected to symmetrical pole-residue fitting by vector fitting [12]. The passivity violations were found to be very small and were easily removed by passivity enforcement via perturbation of residue matrix elements [13]. Since the transformer has an ungrounded tertiary, the use of a mode-revealing transformation [14] was essential to retain the behavior of the small eigenvalue of $\mathbf{Y}_{\text{ext}}$, both during fitting and passivity enforcement.

Fig. 7 shows the eigenvalues of $\mathbf{Y}_{\text{ext}}$ in terms of samples and the extracted model using 120 pole-residue terms. The model extraction is seen to be highly accurate for small and large eigenvalues alike, implying that the model can be applied in a wide range of applications without error magnifications.

Fig. 8 shows a few elements of matrix $\mathbf{J}_1$ (38a), demonstrating the effect of the damping factor and of **F**. The damping factor is seen to give the desired effect of attenuating the resonance peaks. The **F**-matrix does however not have any noticeable affect on the responses of $\mathbf{J}_1$, which represent the voltage transfer from external terminals (with known voltages) to internal nodes. It follows that the significance of **F** is mainly for the terminal behavior of the model as described by $\mathbf{Y}_{\text{ext}}$ since the small eigenvalues of $\mathbf{Y}_{\text{ext}}$ are sensitive to **F**, see Fig. 6.

This article has been accepted for publication in a future issue of this journal, but has not been fully edited. Content may change prior to final publication. Citation information: DOI 10.1109/TPWRD.2018.2847725, IEEE Transactions on Power Delivery

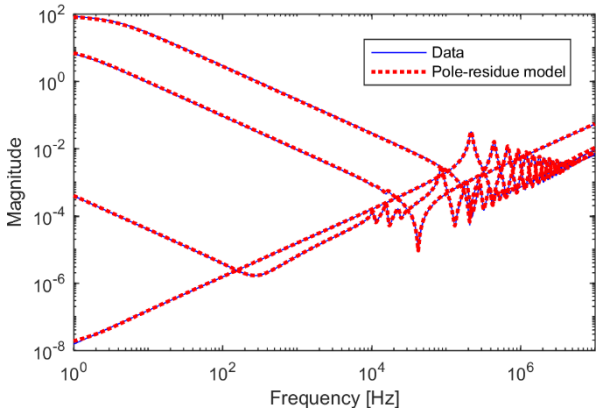

Fig. 7. Eigenvalues of extracted model.

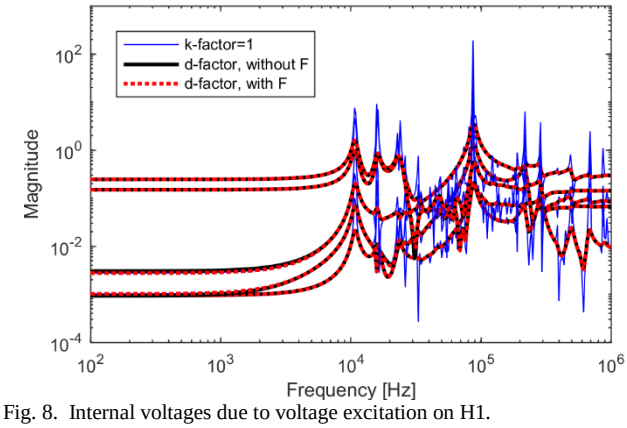

Fig. 8. Internal voltages due to voltage excitation on H1.

VIII. Comparison Against Measurements

Extensive measurements have been performed on this transformer as described in [11], including terminal admittance and voltage transfer.

A. Terminal Admittance in Frequency Domain

Fig. 9 compares the eigenvalues of the model's $\mathbf{Y}_{ext}$ with those of a direct admittance measurement. It is observed that the damping characteristics are reproduced quite accurately except at very high frequencies (above 1 MHz) where the white-box model's spatial discretization starts becoming inadequate and where the measurements are possibly inaccurate. At low frequencies, there is a big deviation in the small eigenvalue that is related to the no-load current. This deviation is in part due to inaccurate measurements since the applied small-signal measurements do not sufficiently excite the steel core to reach the proper magnetization level.

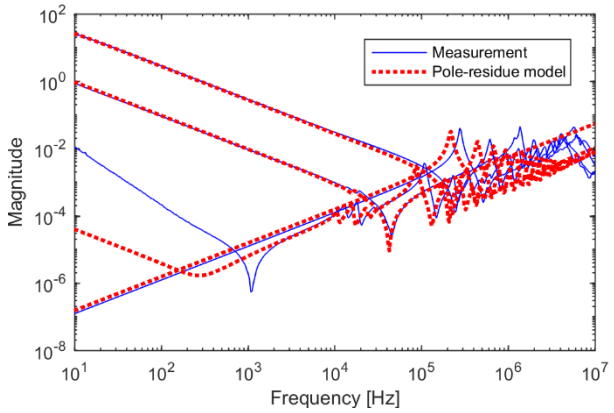

Fig. 9. Terminal admittance matrix eigenvalues.

B. Voltage Transfer in Time Domain

We consider one case where a 1.2/50 µs lightning impulse voltage wave is applied to H1 with X1, Y1 and Y2 open. The voltage responses were obtained via frequency sweep measurements followed by rational fitting and recursive convolution as detailed in [11]. The measured time domain responses are shown in Fig. 10 along with simulated responses by the passive pole-residue model. Fig. 10 also shows the result when losses are represented by DC resistances in the model (*k*-factor=1). It is observed that usage of the damping factor gives a satisfactory representation of the damping of the responses, compliant with the frequency domain result in Fig. 9. The dominating oscillation frequency is about 10% lower in the simulated result, due to inaccuracies in the calculation of the model's parameters (matrices **L** and **C**). Ongoing calculations within CIGRE JWG A2/C4.52 show that for this example, the biggest differences in the natural frequencies are likely to result from the calculation of **C**.

Fig. 11 shows the voltage on three inner points in the regulating winding. These voltages are calculated by the state-space model having external terminal voltages as input, obtained by simulation using the pole-residue model. The simulated result is shown to agree well with the measurement. In this case, the inclusion of the damping factor had only a small effect on the responses in the given time window. The initial part of the measurement is seen to contain a high-frequency oscillation component that is not represented in the white-box model.

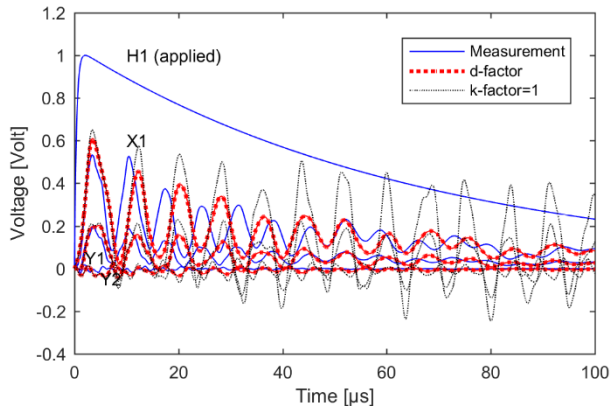

Fig. 10. Measured and simulated voltage transfer from H1 to X1, Y1, Y2.

This article has been accepted for publication in a future issue of this journal, but has not been fully edited. Content may change prior to final publication. Citation information: DOI 10.1109/TPWRD.2018.2847725, IEEE Transactions on Power Delivery

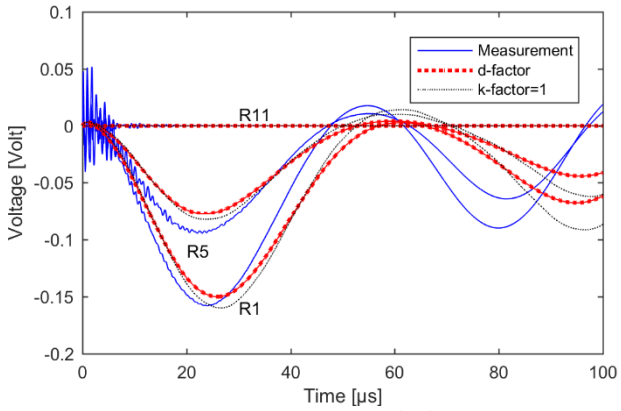

Fig. 11. Measured and simulated voltage transfer from H1 to R1, R5, R11.

C. Voltage Application on LV Terminal

Fig. 12 shows the calculated voltage response on terminals H1, Y1, and Y2 when applying the 1.2/50 µs voltage wave on X1. It is observed that the pole-residue model with inclusion of the damping factor gives a satisfactory representation of the damping of the high-frequency superimposed oscillation.

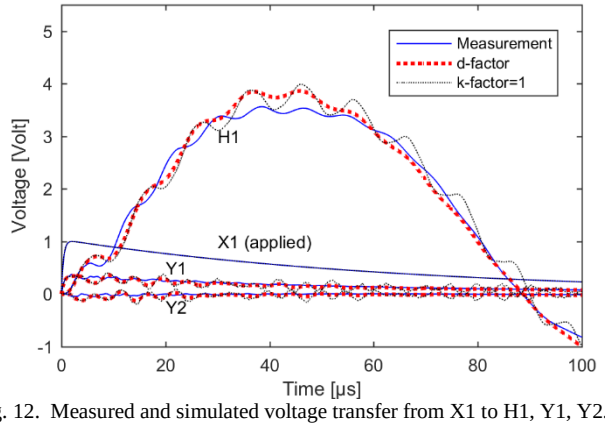

Fig. 12. Measured and simulated voltage transfer from X1 to H1, Y1, Y2.

D. Computation Time

Table III lists the CPU time for an implementation in Matlab. The calculation involves 5001 time domain samples with a state matrix of 432 states. It is observed that the computation time is about one second.

TABLE III
CPU TIME FOR CALCULATING 5000 TIME STEPS.

Step	Time [sec]
Calculate four terminal voltages. (pole-residue model)	0.12
Calculate 213 internal node voltages. (sparse state-space model)	0.95

IX. DISCUSSION

A. Significance of Modifying Input and Output Variables

In the adopted state-space model we modified the formulation by introducing small series resistors to obtain external voltages $\mathbf{v}_{ext}$ as input and external currents $\mathbf{i}_{ext}$ as output (admittance). Without this change, we have $\mathbf{i}_{ext}$ as input and $\mathbf{v}_{ext}$ as output (impedance). With the latter formulation, the use of matrix **F** becomes mandatory. Fig. 13 shows the eigenvalues of $\mathbf{Y}_{ext}$ as calculated from the inverse of $\mathbf{Z}_{ext}$. It is observed that at 50/60 Hz, the large eigenvalues of $\mathbf{Y}_{ext}$ become highly incorrect unless **F** is applied, implying much too large short-circuit impedances in the model. Even with the use of **F**, the resonance peaks at high frequencies are observed to become exaggerated, e.g. at 200 kHz. Table IV shows the effect of the damping factor on 60 Hz parameters.

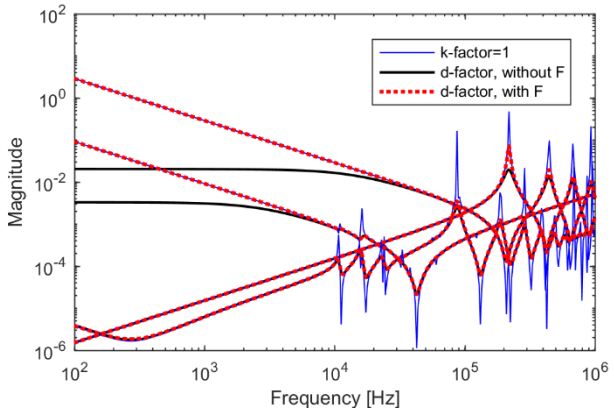

Fig. 13. Eigenvalues of $\mathbf{Y}_{ext}$ by impedance-based model, with and without usage of **F**.

TABLE IV
VOLTAGE RATIOS, SHORT-CIRCUIT IMPEDANCE, OPEN-CIRCUIT LOSSES AND CURRENT. IMPEDANCE-BASED MODEL

	V_S/V_P	V_T/V_P	Z_k [Ω]	P_{oc} [kW]	I_{oc} [A]
Original model	0.300	0.104	1.49+j74.4	34.3	0.93
Model with *d*-factor	0.300	0.101	3466+j151	57.8	0.96
Model with *d*-factor and **F**	0.300	0.104	1.51+j74.4	34.3	0.93
FAT	0.300*	0.104*	1.50+j75.1	33.0	0.32

*Calculated from turns ratio

B. Limiting Information About Internal Node Voltages

The manufacturer could be reluctant to provide a model which gives information about the internal overvoltages. This issue is resolved by providing only a terminal equivalent for the transformer, either by (34) with the first n_1 rows of **CFS**, or by the pole-residue model (34). The manufacturer may additionally give access to any subset of the internal node voltages by providing additional rows in **CFS** (34), or by providing a subset of rows in $\mathbf{J}_1$ (38a) for use with (37a).

C. Damping of Anti-Resonances

The proposed model formulation has two partitions which respectively represent the terminal admittance and the voltage transfer from external terminals to internal nodes. In order for the model to behave reasonably accurate in any situation, one must require that the terminal admittance matrix eigenvalues are accurate in the relative sense. Since the terminal admittance defines the current response to a voltage application, it follows that the admittance resonance peaks must have the correct damping. If the model is to be applied in simulations with some terminals open or lightly loaded, one must in addition require that the anti-resonance points have the correct damping since a part of the admittance matrix is then effectively inverted. The

This article has been accepted for publication in a future issue of this journal, but has not been fully edited. Content may change prior to final publication. Citation information: DOI 10.1109/TPWRD.2018.2847725, IEEE Transactions on Power Delivery

inversion causes the anti-resonances to appear as resonances in the voltage response on the open terminals as explained in Section II.B. It is reassuring that the model seems to give a reasonable damping of also the anti-resonances points as is evident in Fig. 13. The situation is very different in the case of the voltage transfer. Here, only the damping of the resonance peaks is of importance since there is no matrix inversion involved.

D. Damping Factor Scattering

It is important to realize that a model based on empirical damping factors will always have certain limitations in accuracy simply because the scattering of the actual damping around the empirical damping curve is substantial, see Fig. 4. This deficiency will be a problem in simulation of resonant overvoltages where one requires high accuracy for both resonance frequencies and their associated damping. Still, for use in more general simulations where the accuracy requirement of the transformer model is not critical, the use of damping functions can be a very practical approach.

X. Conclusions

We presented a new approach for including an empirical damping factor function in a lumped-parameter type white-box model. The impedance-based state space model that naturally arises is reformulated as a multi-terminal admittance-based model with respect to external terminals. Internal node voltages are optionally calculated from the voltage transfer from external nodes to internal nodes. The undesired change to the model's behavior at lower frequencies caused by the damping factor is mitigated by a correction to the output matrix. The approach was successfully applied to the modeling of a single-phase transformer, showing good agreement between simulated and measured transients in terms of damping of high-frequency oscillations.

XI. Acknowledgement

The authors would like to thank the consortium participants of the SINTEF-led project "ProTrafo" (project no. 207160/E20) for sponsoring this research project. We also thank our colleagues from CIGRE JWG A2/C4.52 for useful discussions.

Appendix

For (29) we can write

$$\begin{aligned}\mathbf{F} &= [s_0\mathbf{I}-\mathbf{A}]^{-1}[s_0\mathbf{I}-\bar{\mathbf{A}}] \\ &= [\mathbf{S}(s_0\mathbf{I}-\boldsymbol{\Lambda})\mathbf{S}^{-1}]^{-1}[\mathbf{S}(s_0\mathbf{I}-\bar{\boldsymbol{\Lambda}})\mathbf{S}^{-1}]\end{aligned} \tag{41}$$

Applying the rule of matrix inverse, $(\mathbf{AB})^{-1}=\mathbf{B}^{-1}\mathbf{A}^{-1}$, gives

$$\begin{aligned}\mathbf{F} &= [\mathbf{S}(s_0\mathbf{I}-\boldsymbol{\Lambda})^{-1}\mathbf{S}^{-1}][\mathbf{S}(s_0\mathbf{I}-\bar{\boldsymbol{\Lambda}})\mathbf{S}^{-1}] \\ &= \mathbf{S}(s_0\mathbf{I}-\boldsymbol{\Lambda})^{-1}(s_0\mathbf{I}-\bar{\boldsymbol{\Lambda}})\mathbf{S}^{-1}\end{aligned} \tag{42}$$

References

[1] R.M. Del Vecchio, B. Poulin, P.T. Feghali, D.M. Shah, and R. Ahuja, *Transformer design principles*, CRC Press, 2010.

[2] W.J. McNutt, T.J. Blalock, R.A. Hinton : "Response of Transformer Windings to System Transient Voltages", *IEEE Trans. Power Apparatus and Systems*,Vol. PAS-93, Issue 2, 1974, pp 457-467.

[3] CIGRE Technical Brochure 577A, "Electrical transient interaction between transformers and the power system. Part 1 – Expertise", CIGRE JWG A2/C4.39, April 2014.

[4] B. Gustavsen and A. Portillo, "Interfacing *k*-factor based white-box transformer models with electromagnetic transients programs", *IEEE Trans. Power Delivery*, vol. 29, no. 6, pp. 2534-2542, Dec. 2014.

[5] B. Gustavsen, A. Portillo, "A black-box approach for interfacing white-box transformer models with electromagnetic transients programs", IEEE PES GM 2014, Washington DC, July 27-31, 2014, 5 p.

[6] A. Semlyen, F. De León: "Eddy current add-on frequency dependent representation of winding losses in transformer models used in computing electromagnetic transients", *IEE Proc.Gener.Transm.Distrib*., Vol.141, N°3, May 1994, pp 209-214

[7] P. I. Fergestad and T. Henriksen, "Transient oscillations in multiwinding transformers," *IEEE Trans. Power App. Syst.*, vol. PAS-93, no. 2, pp. 500–509, Mar. 1974.

[8] S. Grivet-Talocia and B. Gustavsen, *Passive Macromodeling: Theory and Applications*, John Wiley and Sons, 2015.

[9] B. Gustavsen and H.M.J. De Silva, "Inclusion of rational models in an electromagnetic transients program – Y-parameters, Z-parameters, S-parameters, transfer functions", *IEEE Trans. Power Delivery*, vol. 28, no. 2, pp. 1164-1174, April 2013.

[10] Y.M. Zheng and Z.J. Wang, "Determining the broadband loss characteristics of power transformer based on measured transformer network functions and vector fitting method", *IEEE Trans. Power Delivery*, vol. 28, no. 4, pp. 2456-2464, October 2013.

[11] B. Gustavsen, A. Portillo, R. Ronchi, A. Mjelve, "Measurements for validation of manufacturer's white-box transformer models", Procedia Engineering 202 (2017), pp. 240-250.

[12] B. Gustavsen, and A. Semlyen, "Rational approximation of frequency domain responses by vector fitting", *IEEE Trans. Power Delivery*, vol. 14, no. 3, pp. 1052-1061, July 1999.

[13] B. Gustavsen, and A. Semlyen, "Enforcing passivity for admittance matrices approximated by rational functions", *IEEE Trans. Power Systems*, vol. 16, no. 1, pp. 97-104, Feb. 2001.

[14] B. Gustavsen, "Rational modeling of multi-port systems via a symmetry and passivity preserving mode-revealing transformation", *IEEE Trans. Power Delivery*, vol. 29, no. 1, pp.199-205, February 2014.

Biographies

Bjørn Gustavsen (M'94–SM'2003–F'2014) was born in Norway in 1965. He received the M.Sc. degree and the Dr. Ing. degree in Electrical Engineering from the Norwegian Institute of Technology in Trondheim, Norway, in 1989 and 1993, respectively. Since 1994 he has been working at SINTEF Energy Research, currently as Chief Research Scientist. His interests include simulation of electromagnetic transients and modeling of frequency dependent effects. He spent 1996 as a Visiting Researcher at the University of Toronto, Canada, and the summer of 1998 at the Manitoba HVDC Research Centre, Winnipeg, Canada. He was Marie Curie Fellow at the University of Stuttgart, Germany, August 2001–August 2002. He is convenor of CIGRE JWG A2/C4.52.

Álvaro Portillo(M'84–SM'2001) was born in Uruguay in 1954. He graduated in Electrical Engineering in the Uruguay University in 1979. He worked in the Uruguayan electrical utility (UTE) up to 1985 in activities related with transformers acceptance, installation and maintenance. From 1985 to 1999 he worked in MAK (Uruguayan manufacturer of transformers), from 2000 to 2007 as consultant in TRAFO (Brazilian manufacturer of transformers) and from 2007 up today as consultant in software tools development for transformer design at WEG (Brazilian manufacturer of transformers). He is a professor at the Uruguayan Republic University since 1977, now responsible for all post-graduation courses about transformers and also work as consultant of electric utilities in the elaboration of technical specifications and design review of power transformers. He is a task force leader within CIGRE JWG A2/C4.52.